Biosensors and Bioelectronics 143 (2019) 111642

Contents lists available at ScienceDirect

Biosensors and Bioelectronics

journal homepage: www.elsevier.com/locate/bios

Label-free electrochemical impedimetric immunosensor for sensitive detection of IgM rheumatoid factor in human serum

Somasekhar R. Chinnadayyala[a], Jinsoo Park[a,b], Muhammad A. Abbasi[a], Sungbo Cho[a,b,*]

[a] Department of Electronics Engineering, Gachon University, Seongnam-si, Gyeonggi-do, 13120, South Korea
[b] Gachon Advanced Institute for Health Science & Technology, Gachon University, Incheon, 21999, South Korea

ARTICLE INFO

Keywords:
Interdigitated wave type microelectrode array
Self-assembled monolayers
IgM rheumatoid factor
Atomic force microscopy
Electrochemical impedance spectroscopy

ABSTRACT

The authors report a label-free and direct detection of rheumatoid factor- Immunoglobulin M (IgM-RF) based on an impedimetric-interdigitated wave type microelectrode array (IDWμE). IDWμE was functionalized with a self-assembled monolayer (SAM) of thioctic acid for antigen immobilization. The SAM functionalized IDWμE were characterized by atomic force microscopy, Energy Dispersive X-Ray Spectroscopy, and X-ray photoelectron spectroscopy. The covalent immobilization of IgG-Fc onto the SAM modified electrode arrays was characterized morphologically via AFM and electrochemically via cyclic voltammetry and electrochemical impedance spectroscopy. Impedimetric measurements in the presence of redox probe (Potassium ferrocyanide and potassium ferricyanide) showed a significant change in both the impedance spectrum and charge transfer resistance upon IgM-RF binding. Impedance measurements were target specific and linear with an increase in IgM-RF concentrations between 1 and 200 IU mL^{-1} in redox probe and human serum, respectively. The sensor showed detection limits of 0.6 IU mL^{-1} in the presence of redox probe and 0.22 IU mL^{-1} in the human serum. The biosensor exhibited good reproducibility (relative standard deviation (RSD), 4.96%) and repeatability (RSD, 2.31%) with an acceptable selectivity towards IgM-RF detection. The sensor also showed a good stability for 3 weeks at 4 °C in 1X PBS. Therefore, the sensitive and stable immunosensor exhibiting IDWμE features can be integrated with a miniaturized potentiostat to develop a sensing system that detects IgM-RF for point-of-care applications.

1. Introduction

Rheumatoid arthritis (RA) is a progressive and chronic inflammatory autoimmune condition that causes deformity of joints and pain in aged populations (Smolen et al., 2018). It is the most common autoimmune disease, affecting nearly 1% of the world's population (Myasoedova et al., 2010). RA arises as a result of immune dysfunction, in which the modified self-epitopes themselves act as the targets of autoantibodies (AAb) generated by the host immune system (Campuzano et al., 2019). Studies have recognized some of the causal pathways and target proteins that lead to AAb generation in RA (Sweet et al., 2013). The AAb commonly detected in the serum of RA patients consist of rheumatoid factors (RF) and anti-citrullinated peptide antibodies (ACPAs) (Trier et al., 2018; Aletaha et al., 2010). RF primarily consist of IgM, IgA, and IgG antibodies directed against the Fc fragment within the patient's own IgG antibody molecules (Aletaha et al., 2010; Westwood et al., 2006). The reference level of rheumatoid factor in human serum ranges from 15 to 20 IU mL^{-1} (Aletaha et al., 2010; Murphy et al., 2017; Veigas et al., 2019). The IgM isotype (IgM RF) exhibits the most prevalence in RA diagnosis owing to their polyvalency and are more efficient in agglutination reactions (Bas et al., 2002). The sensitive detection of IgM-RF is in great need for the diagnosis, progression, and early prediction of RA (de Brito Rocha et al., 2019; Ingegnoli et al., 2013). Several classical methods have been used to detect RF, including enzyme-linked immunosorbent assay (ELISA) (Trier and Houen, 2019), agglutination tests (e.g., latex agglutination test (LAT) and hemagglutination test) (Ingegnoli et al., 2013), colorimetric immunoassays (Veigas et al., 2019), immunonephelometry (Sieghart et al., 2018), turbidimetry assays (Falkenburg et al., 2018), fluoroimmunoassay (Knijff-Dutmer et al., 2002) and quartz crystal microbalances (Drouvalakis et al., 2008). Although agglutination reactions are simple and rapid diagnostic assays, they exhibit considerable day-to-day variability, have higher limit-of-detection, and do not provide quantitative results. On the other hand, ELISA is expensive and

* Corresponding author. Department of Electronics Engineering, Gachon University, 1342 Seongnamdaero, Sujeong-gu, Seongnam-si, Gyeonggi-do, 13120, South Korea.
E-mail address: sbcho@gachon.ac.kr (S. Cho).

https://doi.org/10.1016/j.bios.2019.111642
Received 10 June 2019; Received in revised form 26 August 2019; Accepted 27 August 2019
Available online 28 August 2019
0956-5663/

is known to demonstrate false positive or false negative results. Furthermore, analyte contamination of the quartz crystal surface in QCM sensors is not easily avoided from previous measurements. Despite these obstacles, efforts are still being made to improve the sensitivity, dynamic range, reliability, cost, and measurement speed of such analytical methods. Recently, a highly pH-sensitive EIS-YbTixOy (electrolyte-insulator-semiconductor)-based biosensor was reported for the detection of serum RF (Pan et al., 2015).

The fabrication of AAb biosensors, particularly for the diagnosis and monitoring of diseases that exhibit an inflammatory nature, is currently a fast developing research activity. Despite the significant advances in multianalyte detection, sensitivity, and point-of-care (POC) testing provided by these analytical tools, only a few sensing platforms, particularly using electrochemical biosensors, are thus far available for RF detection. A few commercial qualitative and quantitative RF assay kits from various companies, such as Biomatic (15.6–1000 mIU mL^{-1}), Immco (6–50 IU mL^{-1}), Sigma (0–50 IU mL^{-1}), Diamedix (100 IU mL^{-1}), Inova (6.25–100 IU mL^{-1}), Rheumajet RF (BioKit), and Latex RF rapid test kits (Cardinal Health) (qualitative and semi-quantitative LAT) are currently available in the market. RF titer increment in human serum during disease progress is used to provide prognostic, diagnostic, and therapeutic information, which still remains to be properly demonstrated. Therefore, the sensitive quantification of IgM-RF with significant dynamic ranges, selectivity, and sensitivity using rapid, reliable, and precise analytical methods for clinical diagnosis is an important objective.

Notably, electrochemical impedimetric immunosensing using micro/nanoelectrodes has been adopted for fast, selective, and ultrasensitive detection of target protein biomarkers (Yagati et al., 2016, 2018). Furthermore, introduction of nano/microelectrodes and miniaturized sensing transducers into electrochemical sensor fabrication has also been shown to improve detection performance (Fernandes et al., 2014). Interestingly, the micro-fabrication industry has demonstrated immense capabilities in fabricating microelectrodes that are extremely sensitive with lower detection limits and significant dynamic ranges. The fabrication of a simple electronic circuitry for electrochemical IgM-RF quantification along with low-cost manufacturing has made the current electrochemical immunosensing study competitive with other immunosensing techniques.

Self-assembled monolayers offer the simplest ways to produce reproducible, ultrathin, ordered, and oriented monolayers that can retain the activity of biomaterials. Monolayers that are instinctively made from sulfur-containing compounds in contact with metallic surfaces (gold or silver) provide an appropriate platform for biomolecule immobilization. The attachment of proteins/antibodies to the carboxylic end functional groups of self-assembled monolayer (SAM)-forming compounds using carbodiimide activation, in combination with succinimide, is the most commonly applied method for electrochemical biosensor fabrication. The preference placed on hexacyanoferrate [$Fe(CN)_6^{4-/3-}$] as a redox probe in the present study is due to the fast kinetics of thioctic acid (TA) induced by the hydrophilicity of the monolayers, which became slower with the increasing hydrophobicity of the film facilitated by the covalent coupling of biomolecules and target analyte interactions (Cordoba-Torres et al., 2015).

Here, we fabricated an electrochemical impedimetric immunosensor by immobilizing RF antigens onto a thioctic acid- functionalized self-assembled monolayer (TA-SAM) interdigitated wave type microelectrode array (IDWμE). As a proof-of-concept, a human IgG-Fc fragment was selected as the model immobilizing antigen to detect IgM-RF by probing the charge transfer resistance (R_{ct}), which is an interfacial property of electrodes in electrochemical impedance spectroscopy (EIS). The sensor was scaled down (3.5 × 14 mm) and can be integrated to develop a portable immunosensing system to detect IgM-RF for POC applications. The BSA/IgG-Fc/TA-SAM/IDWμE immunosensor detected IgM-RF within 10 min. Furthermore, the SAM of TA-modified microelectrode surfaces offered an appropriate sensing platform for IgM detection and properly preserved the biological activity of the immobilized IgG-Fc. Based on the available information, this is the first report on interdigitated wave type microelectrode configuration for IgM-RF detection in PBS and human serum samples. Moreover, the EIS results suggest the usefulness of the TA-SAM microelectrode structures in designing miniaturized and portable nanobiosensors in the near future.

2. Experimental

2.1. Chemicals and reagents

Rheumatoid factor antibody (IgM; ≥ 95%, 1428 IU mL^{-1}) and rheumatoid factor antigen (human Fc fragment of IgG, IgG-Fc; 90%, 1.760 mg mL^{-1}) were purchased from EastCoast Bio (North Berwick, USA) and Arotec Diagnostics (Wellington, New Zealand), respectively. Thioctic acid (99.9%) was procured from EDQM (Strasbourg, France). Potassium ferrocyanide ($K_4[Fe(CN)_6] \cdot 3H_2O$), potassium ferricyanide ($K_3[Fe(CN)_6]$), and human serum were procured from Sigma-Aldrich (USA).

Phosphate-buffered saline (PBS- containing 137 mM NaCl, 2.7 mM KCl, 4.3 mM Na_2HPO_4, and 1.4 mM KH_2PO_4; pH 7.4) and PBS containing 0.05% Tween-20 and 0.5% BSA were procured from Tech and Innovation (Gangwon, South Korea). Buffer solutions were prepared using deionized water (DI; 18.2 MΩ cm) provided by Purescience (Jungwon, South Korea). All other chemicals were of analytical reagent grade and used straight away without any further purification.

2.2. Fabrication of the IDWμE array

For the impedimetric detection of IgM-RF, a gold-based IDWμE array on a glass slide substrate (3.5 × 14 mm) was fabricated using microfabrication technology. The conductive Ti and Au (thickness: 25 and 50 nm, respectively) layers were deposited via electron beam evaporation and the sensing area of the IDWμE array, which has 7 μm of spacing and width, was patterned via photolithography and a chemical wet etching process. Furthermore, a 96-well polystyrene cell culture plate with a well capacity of 400 μL was used as an electrolyte reservoir for impedance spectra measurement and as a homemade adapter to connect the conductive IDWμE array pads to the potentiostat (Fig. S1).

2.3. Formation of self-assembled monolayers

The electrode arrays were cleaned in successive solutions of acetone, ethanol, and water for 2 min via ultra-sonication, rinsed with DI water, and purged under a low stream of N_2 gas. To immobilize TA-SAM, the electrode arrays were immersed in 10 mM TA in ethanol (99.5%) for 12 h. After the SAM modification, all TA/IDWμEs were extensively rinsed with 70% ethanol followed by DI water to remove unbound thiol moieties. To remove H-bonded thiol, additional rinsing was performed by placing the substrate in fresh absolute ethanol, followed by sonication for 2 min. Immediately after sonication, the electrodes were again rinsed extensively with 70% ethanol and DI water and then blown dry with N_2 gas.

2.4. Atomic force microscopy (AFM) and Energy Dispersive X-Ray Spectroscopy (EDX)

AFM was carried out using an ambient air scanning probe microscope (XE–100 Park ystems, South Korea). Images were recorded via a typical non-contact mode using the XEP software. The elemental analysis was done using a scanning electron microscope (HITACHI S-4700, Japan) equipped with HORIBA EX 250.

2.5. X-ray photoelectron spectroscopy

X-ray photoelectron spectroscopy (XPS) measurements were carried out using a Thermo Electron Corporation (Waltham, Massachusetts, US) spectrometer with a monochromatic Al K_α X-ray source. Survey spectra were first recorded and region scans were then conducted over the S (2p) and C(1s) photoelectron binding energy regions. A 200 eV pass energy, 1 eV step size, 50 ms dwell time, and 400 μm × 400 μm X-ray spot size were used for a survey scan (range = 1200 to −5 eV). Region scans (Au 4f, C 1s, S 2p, O1s) exhibited typical bandwidths of 15–20 eV, 50 eV pass energies, 1 eV step sizes, and 50 ms dwell times. All XPS spectra were analyzed using a standard Gaussian curve fit with Shirley background subtraction (Longo et al., 2015).

2.6. Preparation of the IgM-RF bioelectrode

To covalently immobilize human IgG-Fc fragments (50 μg mL^{-1}) onto TA-activated surfaces, 10 μL (50 μg) of the human IgG-Fc fragment solution was dropped onto the electrode chip surface and then kept in a humid chamber for 1 h to prevent the electrode surface from drying during the binding process. The human IgG-Fc fragments were immobilized by a covalent coupling reaction between the amino group of IgG-Fc fragments and the reactive succinimidyl group of the TA-SAM on the electrode surface. The electrodes (IgG-Fc/TA-SAM/IDWμEs) that formed were thoroughly washed with 1X PBS to remove any unbound IgG-Fc fragments. Finally, to block non-specific binding, the electrodes were washed thoroughly with 1 × PBS containing 0.05% Tween-20 and 0.5% BSA for 2 min, thus forming BSA/IgG-Fc/TA-SAM/IDWμEs. According to the World Health Organization reference RF serum, IgM-RF concentrations can be expressed as IU mL^{-1}. Next, different amounts of IgM-RF were mixed into 10 mM of PBS (pH 7.4) or human serum to obtain final concentrations of 1, 10, 50, 100, and 200 IU mL^{-1}. Fresh solutions were prepared for each experiment.

2.7. Electrochemical measurements

2.7.1. Cyclic voltammetry

Electrochemical measurements were carried out using an IVIUM CompactStat potentiostat (Eindhoven, Netherlands) with bare and modified IDWμE array containing a pair of gold conductive pads that acted as the working/sensing electrodes and counter/reference electrodes, respectively. (Fig. 1). Cyclic voltammetry (CV) was performed with an IVIUM CompactStat potentiostat (Eindhoven, Netherlands) in a background solution of 5 mM $K_3Fe(CN)_6/K_4Fe(CN)_6$ (1:1) in 1X PBS (10 mM, Phosphate buffered saline) (pH 7.4). The CV scans were measured in a potential window of +0.5 V to −0.5 V, and at a scan rate of 50 mV s^{-1}. A three-electrode system was employed with platinum coil as counter electrode, Ag/AgCl (saturated NaCl) as reference electrode, and bare IDWμE array or modified IDWμE arrays as the working electrode.

2.7.2. Electrochemical impedance spectroscopy

Impedance analysis of the modified electrodes was carried out in a background solution of 5 mM $K_3Fe(CN)_6/K_4Fe(CN)_6$ (1:1) in 1X PBS, using an input potential of 50 mV amplitude that scanned over the 1–100,000 Hz frequency range with an increment of 5 frequencies for each decade. Prior to the experiments, all electrolyte solutions were deoxygenated by bubbling with pure N_2 gas and all the experiments were performed at room temperature (25 °C). The impedance fitting was carried out by an equivalent circuit model to the measured impedance spectra using a non-linear curve fitting software (ZView; Scribner Associates Inc., Southern Pines, USA). A pH of 7.4 was chosen for all of the electrochemical response studies of the immunosensors as it was the recommended pH for biomolecules to initiate higher biological activity. The immobilization of TA-SAM, immobilization of IgG-Fc onto the electrode arrays, and immunosensor development process along with the underlying working principle are shown in Fig. 1.

3. Results and discussion

3.1. Characterization of TA self-assembled monolayers

EDX measurements were performed to confirm SAM layer immobilization on the electrode surface by studying the elemental composition of the electrode after SAM treatment. The detailed explanation of the EDX spectra were presented in suppl. material (Fig. S2). The efficiency of SAM immobilization and the nature of thiol-gold interactions are further verified using XPS. To understand the nature of SAM–Au interaction, focusing on the contributions of the sulfur atoms and the carbon atoms, S 2p and C 1s XPS bands of which are reported in Fig. S4 b and c, respectively. The detailed explanation of the XPS spectra were presented in suppl. material (Fig. S4).

3.2. Morphological characterization of the fabricated bioelectrode

AFM topology images were recorded to study the morphological characteristics of the electrode surface after each major IDWμE fabrication step. Fig. 2a shows the polycrystalline surface of the bare gold IDWμE with an average roughness of 1.95 nm. The electrode surface after TA-SAM immobilization was transformed into a homogenous, densely-packed aligned structure with a smooth surface topography and an average roughness of 1.06 nm when compared to the bare gold IDWμE (Fig. 2b). The electrode surface modified with the IgG-Fc/TA-SAM film was changed into a particle structure, which reflected the successful immobilization of protein antibodies on the surface, with a 3.72-nm increase in average roughness (Fig. 2c). After IgM-RF bound onto the BSA/IgG-Fc/TA-SAM/IDWμE surface, a clear protrusion topography across the whole electrode surface was formed due to stable immunocomplex formation with a 5.03-nm rise in surface roughness (Fig. 2d).

3.3. Electrochemical characterization of the fabricated bioelectrode

3.3.1. Cyclic voltammetry

Cyclic voltammetry (CV) of the bare Au-IDWμE array and modified Au-IDWμE arrays was determined using a solution of 5 mM $K_3Fe(CN)_6/K_4Fe(CN)_6$ (1:1) in 1X PBS to record the changes in electrochemical behavior introduced at different stages of electrode modification (Fig. S3). The CV of the bare IDWμE show an electrochemical response for $Fe(CN)_6^{4-/3-}$ with an oxidation and reduction peak as expected (Fig. S3, *curve i*). After the electrode was functionalized with TA-SAM (TA-SAM/IDWμE), the CV curve altered drastically and the peak currents of the TA-SAM/IDWμE decreased dramatically when compared to those of IDWμE (Fig. S3, *curve ii*). The effect possibly rises due to the formation of a very high degree of the SAM insulation layer, which results in the hindrance of the $[Fe(CN)_6]^{3-/4-}$ ion transport towards the electrodes. Furthermore, the CV of EDC-NHS/TA-SAM/IDWμE (Fig. S3, *curve iii*) shows a clear oxidation and reduction peak when compared to TA-SAM layer due to the formation of neutral amine bonds between the terminal carboxyl groups of SAM and EDC/NHS, thus allowing ions to move towards the modified EDC-NHS/TA-SAM electrode. Moreover, IgG-Fc-modified electrodes (Fig. S3, *curve iv*) show reduced ferricyanide response and distended peak-to-peak separation, which suggests that an insulating biomolecular layer of IgG-Fc was immobilized onto the electrode surface.

3.3.2. Electrochemical impedance spectroscopy (EIS)

EIS was used to characterize the interfacial properties on the electrode surface during electrode fabrication and response studies of the electrode using different IgM-RF concentrations. Fig. 3a and b shows the impedance spectra, presented as bode plots (Z vs –Φ), on differently modified electrodes using a solution of 5 mM $K_3Fe(CN)_6/K_4Fe(CN)_6$

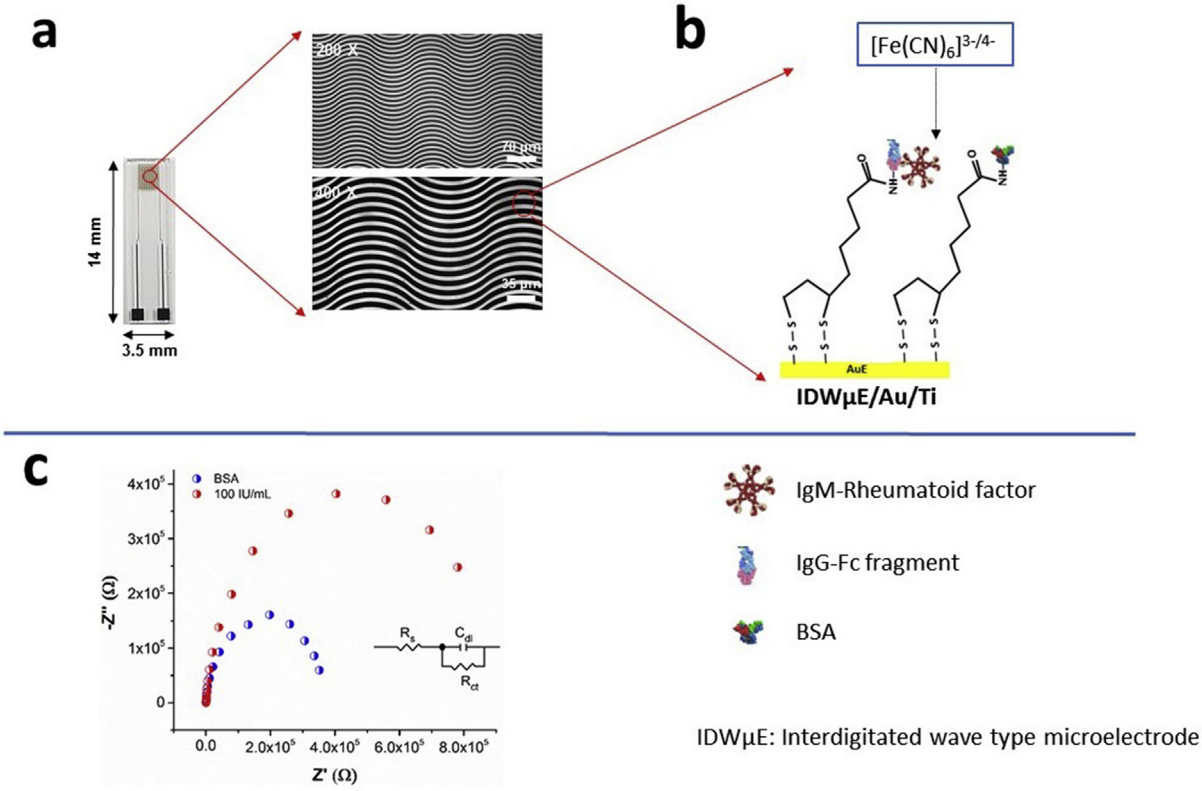

Fig. 1. Photograph of the fabricated IDWµE with dimensions of 3.5 × 14 mm. Both low (200×) and high (400×) magnification microscopic images of the IDWµE array show a finger width and spacing of 7 µm (**a**). Schematic representation of SAM functionalization on IDWµE and crosslinking of IgG-Fc fragments onto the functionalized electrode array (**b**). The sensing mechanism of the impedimetric immunosensor based on the R_{ct} measured from the high frequency semicircles of the impedance spectra after immobilizing TA-SAM, IgG-Fc fragments, BSA, and IgM-RF (where, C_{dl}, double layer capacitance; R_{ct}, charge transfer resistance; R_s, solution resistance) (**c**).

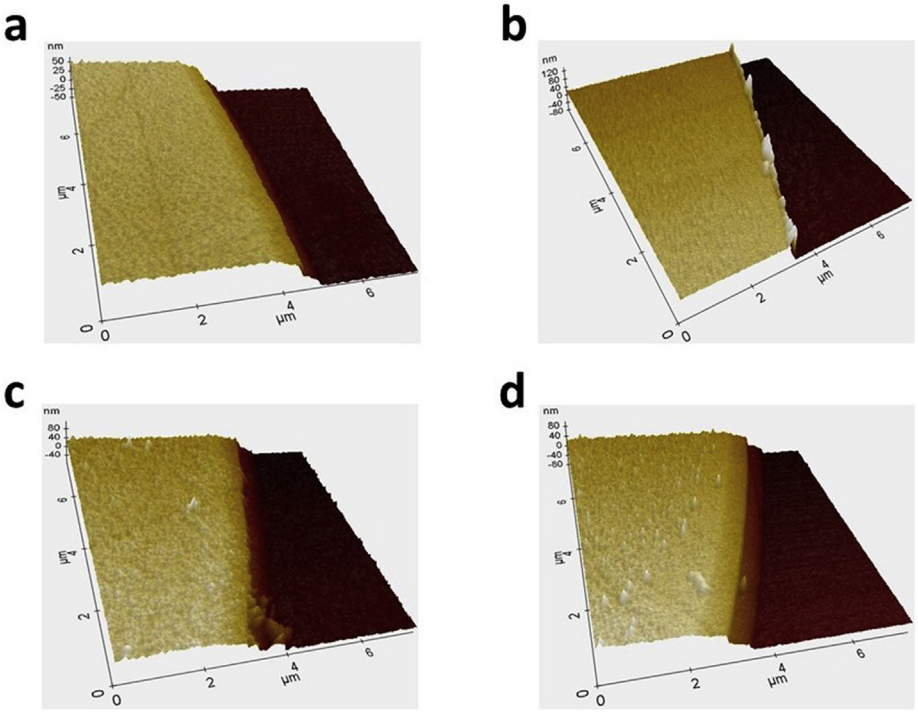

Fig. 2. AFM images of the bare IDWµE (**a**), TA-SAM/IDWµE (**b**), IgG-Fc/EDC/NHS/TA-SAM/IDWµE (**c**), and IgM-RF/BSA/IgG-Fc/TA-SAM/IDWµE (**d**).

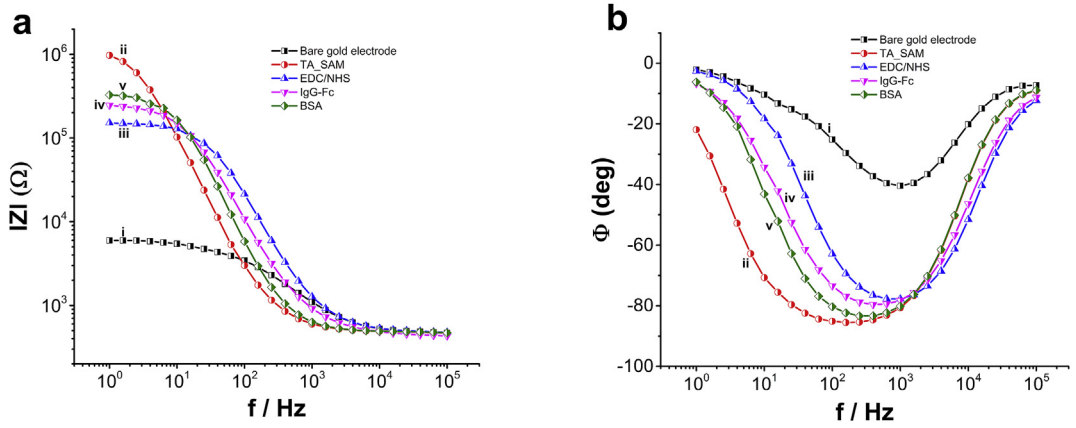

Fig. 3. Bode plot of the impedance magnitude (|Z|) (**a**) and phase (–Φ) (**b**) at different modification stages of the IDWμE array surface in order to detect IgM-RF in 5 mM $K_3Fe(CN)_6/K_4Fe(CN)_6$ (1:1) in 1X PBS solution (pH 7.4).

(1:1) in 1X PBS. From the Bode plots in Fig. 3a *curve i*, the bare IDWμE array mainly showed three distinct regions in the impedance magnitude (|Z|) that were consistent with double layer capacitance (mid-frequency region), charge transfer resistance (low frequency region) with the highest value of |Z|, and solution resistance (high-frequency region). An equivalent circuit model (Randles circuit) was also assumed and fitted with the impedance spectra measured from the electrodes, as shown in the inset of Fig. 3a. At frequencies higher than 10 kHz, the total impedance of the system was governed by the ohmic resistance of the electrolyte solution (R_S) and parasitic impedance. In the measured frequency range, the electrode interfacial impedance was in parallel with the R_{ct}.

Furthermore, the capacitive electrode interfacial impedance is represented as a constant phase element (CPE) of measured impedance i.e., $1/[CPE-T\cdot(i\omega)^{CPE-P}]$ (where, *i* and *ω* are the imaginary unit and angular frequency of the sinusoidal signal, respectively) (Vyas et al., 2010). The parameters of the Randles circuit model (Selvaprakash and Chen, 2014), determined by fitting the measured impedance spectra, are shown in Table S1. The changes in the measured impedance magnitude (|Z|) after the modification process on the IDWμE array surface affected the R_{ct} and C_{dl} of the electrode. The TA-incubated electrode showed a larger |Z| value, which indicated a greater extent of SAM functionalization on the electrode surface and resulted in the blocking of the $[Fe(CN)_6]^{3-/4-}$ ion transport towards the electrode surface (Fig. 3a, *curve ii*). After EDC-NHS activation, the measured |Z| value decreased because of the binding reaction between EDC-NHS and the SAM carboxylic terminal functional group, which resulted in the formation of neutral amine bonds that facilitated ion transfer towards the EDC/NHS modified electrode (Fig. 3a, *curve ii*). The immobilization of IgG-Fc fragments (50 μg mL^{-1}) and BSA (0.5%) onto the EDC/NHS-activated SAM electrode further led to an increased |Z| value at lower frequencies (Fig. 3a, *curve iv* and *curve v*). Notably, the crosslinking of biomolecules onto the electrode surface is suspected to obstruct the tunelling of the redox coulple towards the sensory platform.

3.4. Electrochemical response characteristics of the IgM-RF/BSA/IgG-Fc/TA-SAM/IDWμE bioelectrode

The present IgM-RF electrochemical impedance immunosensor was well reflected in the R_{ct}, which represents the resistance at low frequencies. The results demonstrate that the R_{ct} variations on the modified electrode could be a detection parameter for the sensitive determination of IgM-RF. This resistance was therefore measured for a wide range of IgM concentrations (from 1 to 200 IU mL^{-1}). To evaluate its response to IgM-RF, the immunosensor was incubated with different concentrations of IgM-RF for 10 min. EIS measurements were then carried out in 5 mM $[Fe(CN)_6{}^{-3/-4}]$. As shown in Fig. 4, R_{ct} values increased with an increase in IgM rheumatoid factor concentrations. The change in R_{ct} values was proportional to the linear increase in IgM-RF concentrations over the 1–200 IU mL^{-1} range (Fig. 4a). The linear regression equation was represented by y = 4415115.5 + 2477.7*x with a correlation coefficient of 0.9983 (Fig. 4b).

Furthermore, the detection limit calculated was 0.6 IU mL^{-1} (S/N = 3). The limit-of-detection (LOD) was determined using (3*SD/sensitivity), where SD represented the standard deviation of the measured impedance signals for the blank and sensitivity represented the slope of the linear calibration curve (Selvaprakash and Chen, 2014). The response studies clearly showed that R_{ct} increased linearly with increasing IgM-RF concentrations. This phenomenon can be described by the formation of a kinetic barrier for electron transfer due to the increase in IgM-RF molecules bound to the immobilized IgG-Fc fragments on the electrode array. The change in R_{ct} of the modified electrode was espoused as a quantification parameter for the sensitive determination of IgM-RF. Thus, R_{ct} was used as the physical signal from the sensor to detect and quantify IgM-RF via specific immunoreactions facilitated on the electrode surface. In this manner, the fabricated immunosensor established proof-of-concept for use in the direct detection of IgM-RF without further amplification of the electrical signal. The sensor showed significant dynamic ranges and detection limits when compared to the other RF biosensors reported earlier in the literature (Table S2.) and with commercially available IgM-RF quantitative ELISA kits, Biomatic (15.6–1000 mIU mL^{-1}), IgM RF (Immco, 6–50 IU mL^{-1}), Sigma (0–50 IU mL^{-1}), Diamedix (100 IU mL^{-1}), Inova (6.25–100 IU mL^{-1}).

3.5. Practical application of the bioelectrode

3.5.1. Interference study

The effect of some agents that interfere with IgM-RF (10 IU mL^{-1}) determination, such as human chorionic gonadotrophin (HCG; 10 IU mL^{-1}), insulin (10 IU mL^{-1}), or tumor necrosis factor-α (TNF-α; 10 IU mL^{-1}), on BSA/IgG-Fc/EDC-NHS/TA-SAM/IDWμE bioelectrode response was studied. These agents, mixed with 1X PBS, were exposed to the bioelectrode separately and their respective EIS spectra were acquired over the 1–100,000 Hz frequency range in $[Fe(CN)_6{}^{3-/4-}]$ solution (Fig. 5a). The results indicated that the response of the bioelectrode was not significantly affected in the presence of these interfering agents in comparison to the control bioelectrode (BSA/IgG-Fc/EDC-NHS/TA-SAM/IDWμE) (Fig. S5), suggesting that the fabricated bioelectrode exhibited high selectivity towards IgM-RF determination.

3.5.2. Storage stability of the bioelectrode

The BSA/IgG-Fc/EDC-NHS/TA-SAM/IDWμE array was taken and R_{ct} variation after IgM-RF addition was measured as a function of time

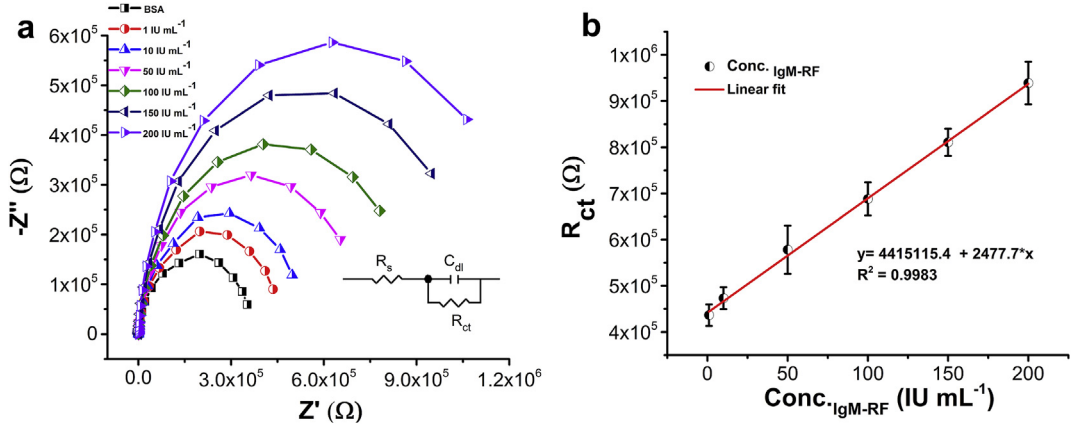

Fig. 4. Impedance response of the BSA/IgG-Fc/TA-SAM/IDWμE array carried out in 5 mM $[Fe(CN)_6^{-3/-4}]$ and measured with respect to the increase in IgM-RF concentrations diluted in 1X PBS (**a**). Linear calibration plot for R_{ct} over increasing IgM concentrations (from 1 to 200 IU mL^{-1}) (**b**). Each data point represents the average of three independent measurements (n = 3). The range is indicated using error bars.

(storage stability). The storage stability of the BSA/IgG-Fc/EDC-NHS/TA-SAM/IDWμE array was determined by measuring the R_{ct} at 10 IU mL^{-1} of IgM-RF over regular intervals of 3 days for about 21 days. Notably, the BSA/IgG-Fc/EDC-NHS/TA-SAM/IDWμE bioelectrode is stored at 4 °C in 1X PBS when not in use. The results confirmed that the bioelectrode retained ~98% of its initial response after 3 weeks (Fig. 5b).

3.5.3. Reproducibility

Furthermore, reproducibility is a crucial factor for clinical application of the immunosensor. Thus, the reproducibility of the immunosensor was tested via intra- and inter-assay relative standard deviations (RSDs). The intra-assay precision of the immunosensor was examined by detecting 10 IU mL^{-1} of IgM-RF in three replicate measurements, whereas the inter-assay precision was evaluated by measuring 200 IU mL^{-1} of IgM-RF in three independently prepared BSA/IgG-Fc/EDC-NHS/TA-SAM/IDWμEs. The intra- and inter-assay RSDs were found to be 4.96% and 2.31% respectively, thereby indicating acceptable levels of immunosensor precision and reproducibility. Good electrode stability is observed due to the covalent coupling of the IgM-RF molecules with the gold surface, which prevents the leakage of biomolecules from the electrode surface. Notably, impedimetric microelectrode-based IgM-RF detection has several advantages over other methods. The detection assay (a) is label-free, (b) is widely applicable, (c) lacks the Warburg diffusion phenomenon, which arises from microfabricated electrodes, (d) has low-cost sample preparation, and (e) is a direct signal readout in the form of an electrical signal.

3.6. Determination of IgM-RF in human serum samples

To demonstrate the practical applicability of the proposed immunosensor, IgM-RF was detected in human serum samples using the BSA/IgG-Fc/EDC-NHS/TA-SAM/IDWμE array. In order to avoid the matrix effects and to construct a robust calibration curve, a diluted solution of the human serum in 1X PBS buffer (1:500) was prepared. Human serum samples containing IgM-RF were applied to the electrode and incubated for 10 min in a humid chamber to react with all available IgG-Fc fragments. After incubation with human serum, EIS measurements were recorded in a 5-mM $[Fe(CN)_6^{-3/-4}]$ electrolyte solution. Compared to the blank, serum sample impedance signals were observed to increase along with an increase in IgM-RF concentrations (Fig. 6a). The concentration of IgM-RF in human serum samples was determined by referring to the calibration curve shown in Fig. 6b. The electrochemical responses determined with human serum samples were dependent on IgM-RF concentrations, thereby demonstrating the absence of matrix interference during IgM detection and suggesting the excellent specificity of the developed impedance sensor. The change in the R_{ct} value was also proportional to the linear increase of IgM-RF concentration over the 10–200 IU mL^{-1} range. The linear regression equation was represented by y = 274,422.6 + 1435.13*x with a correlation coefficient of 0.9941 (Fig. 6b). Furthermore, the LOD calculated was 0.22 IU mL^{-1} (S/N = 3).

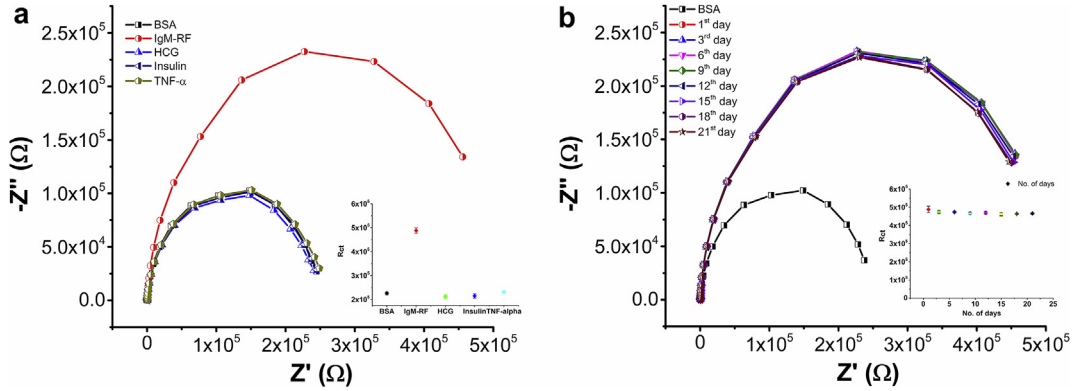

Fig. 5. Selectivity (a) and storage stability (b) of the electrochemical IgM-RF immunosensor in 100 μL of 5 mM $[Fe(CN)6^{-3/-4}]$ in PBS at 10 IU mL^{-1} of IgM-RF concentration. The insets show the change in R_{ct} as a function of the interfering agents (Fig. 5a) and time (Fig. 5b). Each data point represents the average of three values (n = 3). The range is indicated using error bars.

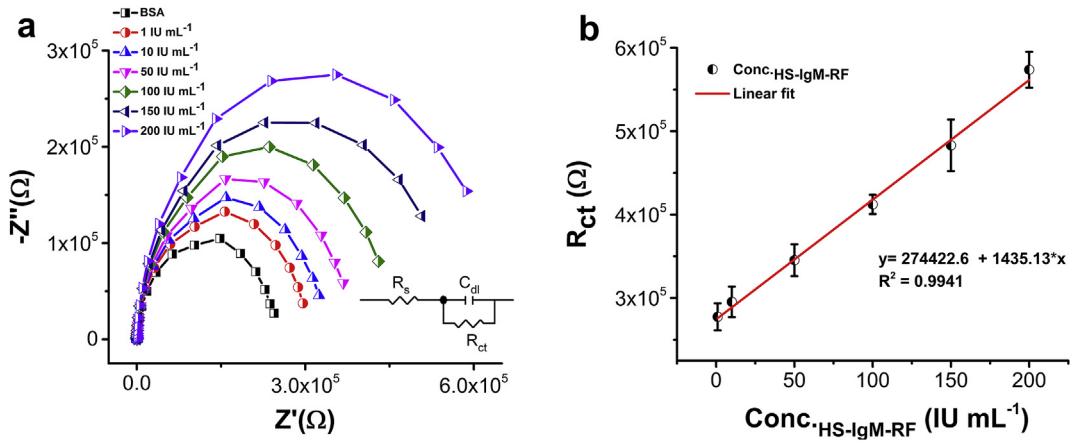

Fig. 6. Impedance response of the BSA/IgG-Fc/TA-SAM/IDWμE array measured with respect to the increase in IgM-RF concentrations diluted in human serum (HS-IgM-RF) (**a**). Linear calibration plot for R_{ct} over increasing human serum diluted IgM-RF concentrations (from 1 to 200 IU mL^{-1}) (**b**). Each data point represents the average of three independent measurements (n = 3). The range is indicated using error bars.

4. Conclusions

Electrochemical impedimetric measurement-based immunosensor for IgM-RF was fabricated via simple immobilization of IgG-Fc fragment antibodies on a TA-SAM/IDWμE array. The formation of TA-SAM on the IDWμE array was confirmed via AFM and EIS. TA-SAM provided a biocompatible environment to immobilize target IgG-Fc fragments while preserving the biological activity of the immobilized IgG-Fc fragments. The covalent coupling of the IgG-Fc fragments on a gold surface provided significant stability to the bioelectrode, which effectively validated its use as an impedimetric biosensor in determining IgM-RF in serum samples. The immunosensor showed a detection limit of 0.60 IU mL^{-1} and a dynamic range of 1–200 IU mL^{-1}. Furthermore, the miniaturized architecture (3.5 × 14 mm) and ability to integrate this sensor with a mini-potentiostat makes it suitable for POC applications in the near future. Notably, the sensor showed limited stability for 3 weeks; thus, efforts should be made to increase the storage stability of the bioelectrode. Moreover, the fabricated bioelectrode is cost-effective as it does not require expensive and sophisticated instruments and fluorescent dyes. It is an adaptable tool that can be applied for disease diagnosis in individuals suspected of developing arthritis, even with RF levels below 1 IU mL^{-1}.

CRediT authorship contribution statement

Somasekhar R. Chinnadayyala: Conceptualization, Methodology, Validation, Formal analysis, Investigation, Writing - original draft. **Jinsoo Park:** Conceptualization, Methodology. **Muhammad A. Abbasi:** Conceptualization, Methodology, Writing - review & editing. **Sungbo Cho:** Conceptualization, Methodology, Resources, Writing - review & editing, Supervision, Project administration, Funding acquisition.

Declaration of competing interest

The authors declare that they have no known competing financial interests or personal relationships that could have appeared to influence the work reported in this paper.

Acknowledgements

This work was supported by grants from the National Research Foundation of Korea, Republic of Korea (grant nos. NRF 2017R1D1A1A09000712, 2018R1C1B6009385, 2018M3A9F1023690, and 2018M3A9F1023691).

Appendix A. Supplementary data

Supplementary data to this article can be found online at https://doi.org/10.1016/j.bios.2019.111642.

References

Aletaha, D., et al., 2010. Ann. Rheum. Dis. 2010 (69), 1580–1588.
Bas, S., Perneger, T.V., Kunzle, E., Vischer, T.L., 2002. Ann. Rheum. Dis. 61, 505–510.
Campuzano, S., Pedrero, M., Gonzalez-Cortes, A., Yanez-Sedeno, P., Pingarron, J.M., 2019. Anal. Methods 11, 871–887.
Cordoba-Torres, P., Mesquita, T.J., Nogueira, R.P., 2015. J. Phys. Chem. C 119, 4136–4147.
de Brito Rocha, S., Baldo, D.C., Andrade, L.E.C., 2019. Adv. Rheumatol. 59, 2–13.
Drouvalakis, K.A., Bangsaruntip, S., Hueber, W., Kozar, L.G., Utz, P.J., Dai, H., 2008. Biosens. Bioelectron. 23, 1413–1421.
Falkenburg, W.J.J., von Richthofen, H.J., Koers, J., Weykamp, C., Schreurs, M.W.J., Bakker-Jonges, L.E., Haagen, I.-A., Lems, W.F., Hamann, D., Schaardenburg, D., Rispens, T., 2018. Clin. Chem. Lab. Med. 56, 1749–1758.
Fernandes, F.C., Santo, s A., Martins, D.C., Goes, M.S., Bueno, P.R., 2014. Biosens. Bioelectron. 57, 96–102.
Ingegnoli, F., Castelli, R., Gualtierotti, R., 2013. Dis. Markers 35, 727–734.
Knijff-Dutmer, E., Drossaers-Bakker, W., Verhoeven, A., van der Sluijs Veer, G., Boers, M., van der Linden, S., van de Laar, M., 2002. Ann. Rheum. Dis. 61, 603–607.
Longo, E., Wright, K., Caruso, M., Gatto, E., Palleschi, A., Scarselli, M., Crescenzi, M.D., Crisma, M., Formaggio, F., Toniolo, C., Venanzi, M., 2015. Nanoscale 7, 15495–15506.
Murphy, D., Mattey, D., Hutchinson, D., 2017. PLoS One 12, 1–11.
Myasoedova, E., Crowson, C.S., Kremers, H.M., Therneau, T.M., Gabriel, S.E., 2010. Arthritis Rheum. 62, 1576–1582.
Pan, T.-M., Lin, T.-W., Chen, C.-Y., 2015. Anal. Chim. Acta 891, 304–311.
Selvaprakash, K., Chen, Y.-U., 2014. Biosens. Bioelectron. 61, 88–94.
Sieghart, D., Platzer, A., Studenic, P., Alasti, F., Grundhuber, M., Swiniarski, S., Horn, T., Haslacher, H., Blüml, S., Smolen, J., Steiner, G., 2018. Front. Immunol. 9, 876.
Smolen, J.S., Aletaha, D., Barton, A., Burmester, G.R., Emery, P., Firestein, G.S., Kavanaugh, A., McInnes, I.B., Solomon, D.H., Strand, V., Yamamoto, K., 2018. Nat. Rev. Dis. Primers. 4, 1–23.
Sweet, R.A., Cullen, J.L., Shlomchik, M.J., 2013. J. Immunol. 190, 1974–1981.
Trier, N.H., Holm, B.E., Heiden, J., Slot, O., Locht, H., Jensen, B., Lindegaard, H., Svendsen, A., Nielsen, C.T., Jacobsen, S., Theander, E., Houen, G., 2018. J. Immunol. Methods 454, 6–14.
Trier, N.H., Houen, G., 2019. In: In: Houen, G. (Ed.), Autoantibodies. Methods in Molecular Biology, vol. 1901 Humana Press, New York, NY.
Veigas, B., Matias, A., Calmeiro, T., Fortunato, E., Fernandes, A.R., Baptista, P.V., 2019. Analyst 144, 3613–3619.
Vyas, R.N., Li, K., Wang, Y.B., 2010. J. Phys. Chem. B 114, 15818–15824.
Westwoodf25, O.M.R., Nelson, P.N., Hay, F.C., 2006. Rheumatology 45, 379–385.
Yagati, A.K., Lee, M.H., Min, J., 2018. Bioelectrochem 122, 93–102.
Yagati, A.K., Park, J., Kim, J., Ju, H., Chang, K.A., Cho, S., 2016. Jpn. J. Appl. Phys. 55, 1–6.